Multigrid Anisotropic Diffusion

Scott T. Acton, *Member, IEEE*

***Abstract*—A multigrid anisotropic diffusion algorithm for image processing is presented. The multigrid implementation provides an efficient hierarchical relaxation method that facilitates the application of anisotropic diffusion to time-critical processes. Through a multigrid V-cycle, the anisotropic diffusion equations are successively transferred to coarser grids and used in a coarse-to-fine error correction scheme. When a coarse grid with a trivial solution is reached, the coarse grid estimates of the residual error can be propagated to the original grid and used to refine the solution. The main benefits of the multigrid approach are rapid intraregion smoothing and reduction of artifacts due to the elimination of low-frequency error. In the paper, the theory of multigrid anisotropic diffusion is developed. Then, the intergrid transfer functions, relaxation techniques, diffusion coefficients, and boundary conditions are discussed. The analysis includes the examination of the storage requirements, the computational cost, and the solution quality. Finally, experimental results are reported that demonstrate the effectiveness of the multigrid approach.**

***Index Terms*—Anisotropic diffusion, image enhancement, PDE methods.**

I. Introduction

ANISOTROPIC diffusion has been widely applied as a mechanism for intraregion smoothing of images. The results of anisotropic diffusion can be used to obtain an enhanced image [14] or as a precursor to higher-level processing such as shape description [15], edge detection [4], image segmentation [3], and object identification and tracking [8]. Although attractive in terms of edge localization and the ability to control scale, anisotropic diffusion may lead to the creation of false edges and false regions, among other ill effects. As with any diffusion technique, processing high-resolution imagery via anisotropic diffusion usually requires a significant number of iterations, precluding real-time processing. Depending upon the realization of the diffusion process, high-frequency error, or noise, can be rapidly eliminated. Even when a well-posed formation of anisotropic diffusion is given, limited relaxation can lead to undesirable artifacts due to low-frequency error. The multigrid approach alleviates the computational cost of the diffusion process and reduces the processing artifacts that can be associated with a reasonable number of iterations.

Continuous-domain diffusion problems described by partial differential equations can be cast in the discrete form (on a finite grid of points). Traditionally, direct methods, such as Gaussian elimination, are applied to achieve a precise solution in a defined number of steps. For some problems, such as the image enhancement and image segmentation tasks defined by anisotropic diffusion, a direct closed-form solution may be difficult to formulate or may be nonexistent. Alternatively, relaxation methods, such as Jacobi and Gauss–Seidel iteration, can be used to obtain approximate solutions. The relaxation schemes iteratively eliminate noise through smoothing, while retaining important region boundaries. Although effective in reducing the high-frequency error, the fine grid relaxation schemes produce low-frequency error in the solution, which may manifest itself as false edges, blotches, or blocky artifacts in the processed image. Given a well-posed formulation such as in [21], these artifacts may be eliminated with a large number of updates (possibly hundreds of iterations), but this may be prohibitive in time-critical applications.

Within the mathematical community, there has been widespread recent interest in multigrid methods [6], [7], [11], [12]. Multigrid techniques have already been used to expedite relaxation problems in image processing [15], [16]. The multigrid methods can be used to provide numerical solutions to the anisotropic diffusion problem. With the multigrid approach, high- and low-frequency error are eliminated rapidly through the use of a multiresolution representation. The original input image provides the initial estimate that can be processed using the standard anisotropic diffusion equations. At the original resolution, only high-frequency error is eliminated quickly, due to the local smoothing of anisotropic diffusion. The error at the finest grid may be estimated at a coarse resolution. Then, the error estimate can then be used to correct the solution. Error correction at coarser resolutions enables the elimination of low-frequency error, since the low frequency error becomes oscillatory at a coarse sampling. Also, relaxation on a coarser grid is less expensive, because there are fewer unknowns, and convergence is improved. The process of computing the residual error on a coarser sampling grid is repeated recursively until a trivial solution can be computed at a very coarse resolution. Then, the error estimates computed at each subsampled grid can be used to correct the results at the next lower (finer) resolution grid, until the original image resolution is reached. This is the essence of the multigrid approach presented here.

In the spirit of multigrid, image pyramids have been used in conjunction with diffusion to improve computational efficiency and solution quality [1]–[3]. The study of multigrid anisotropic diffusion is motivated by the need to add a degree of formalism and analysis to the hierarchical diffusion approach. The pyramid-based algorithms have shown promise in solutions to image enhancement, edge detection, and image segmentation.

Manuscript received July 29, 1996; revised March 10, 1997. This material is based upon work supported by the U.S. Army Research Office under Grant DAAH04-95-1-0255. The associate editor coordinating the review of this manuscript and approving it for publication was Dr. Guillermo Sapiro.

The author is with the School of Electrical and Computer Engineering, Oklahoma State University, Stillwater, OK 74078-0321 USA (e-mail: sacton@master.ceat.okstate.edu).

Publisher Item Identifier S 1057-7149(98)01751-5.

However, the pyramidal approach lacks the rigor the multigrid approach. The two paradigms also have slightly different motivations. Where the pyramid method attempts to use coarse representations to guide enhancement and segmentation at the higher resolution pyramid levels, the multigrid technique reduces the residual error in relaxation at finer representations by coarse grid correction. Thus, the pyramidal algorithms have a spatially intuitive coarse-to-fine strategy, and the multigrid algorithm has an interpretation from the realm of numerical analysis.

The paper first provides the necessary background on anisotropic diffusion. Then, the multigrid approach is discussed, and the multigrid solution for anisotropic diffusion is outlined. The implementation and performance of multigrid anisotropic diffusion are analyzed. Finally, results that demonstrate the efficacy of the multigrid method are presented.

II. Anisotropic Diffusion

The adaptive smoothing of anisotropic diffusion may be implemented by a system of partial differential equations. On a continuous domain, the diffusion equation for image $\boldsymbol{I}$ is given by

$$\frac{\partial \boldsymbol{I}}{\partial t} = \operatorname{div}[\boldsymbol{c}\nabla \boldsymbol{I}] \tag{1}$$

where ∇ is the gradient operator, div is the divergence operator, and $\boldsymbol{c}$ describes the diffusion coefficients [14]. The system of equations has initial condition $\boldsymbol{G}$, which is the initial (possibly corrupted) image. If the elements of $\boldsymbol{c}$ remain constant for all image locations, then isotropic diffusion is enacted. If $\boldsymbol{c}$ is allowed to vary according to the magnitude of the local image gradient, anisotropic diffusion is performed.

Adopting the discrete anisotropic diffusion update in [14], diffusion may be implemented by

$$[I(\boldsymbol{x})]_{t+1} = \left[I(\boldsymbol{x}) + (1/\Omega) \sum_{d=1}^{\Omega} c_d(\boldsymbol{x}) \nabla I_d(\boldsymbol{x}) \right]_t. \tag{2}$$

Here, $\boldsymbol{x}$ represents the coordinates of the M-dimensional discrete domain, Ω is the number of directions in which diffusion is computed, $I(\boldsymbol{x})$ is the intensity at location $\boldsymbol{x}$, $\nabla I_d(\boldsymbol{x})$ is the directional derivative in direction d at location $\boldsymbol{x}$, and time (in iterations) is given by t.

In one dimension (with $\Omega = 2$ directions of diffusion), the discrete anisotropic diffusion equation may be given as

$$\begin{aligned}[I(x)]_{t+1} = \{ & I(x) + (1/\Omega)[c_E(x)\nabla I_E(x) \\ & + c_W(x)\nabla I_W(x)]\}_t \end{aligned} \tag{3}$$

and, in two dimensions, the corresponding equation [14] is

$$\begin{aligned}[I(x,y)]_{t+1} = \{ & I(x,y) + (1/\Omega)[c_N(x,y)\nabla I_N(x,y) \\ & + c_S(x,y)\nabla I_S(x,y) + c_E(x,y)\nabla I_E(x,y) \\ & + c_W(x,y)\nabla I_W(x,y)]\}_t. \end{aligned} \tag{4}$$

$\Omega = 4$ is typically used for two-dimensional (2-D) diffusion, although more elaborate definitions of connectivity are possible. The terms in (3) with subscripts E and W correspond to the two directions of diffusion in the 2-D case. Likewise, the subscripts in (4) correspond to the four directions of diffusion (north, south, east, and west) w.r.t. the location (x, y). Each diffusion coefficient and gradient term are computed in the same manner. For example, in the "northern" direction, the gradient can be defined as a simple difference ($\nabla I_N(x,y) = I(x, y+1) - I(x,y)$), and $c_N(x,y)$ is typically a function of $\nabla I_N(x,y)$.

The multigrid anisotropic diffusion method is not limited to any single realization of the diffusion coefficient. For completeness, the performance of the fixed-resolution and multigrid methods are evaluated using three different solutions for the diffusion coefficient (presented in Section IV), which essentially represent three different classes of anisotropic diffusion techniques. For a comparison of several implementations of the diffusion coefficient, see [20].

III. Multigrid Anisotropic Diffusion

A. The Multigrid Approach

The marriage between multigrid methods and problems defined by partial differential equations has been profitable. The multigrid approach has been extended from simple finite difference problems to include finite element/volume problem, nonlinear problems, and time-dependent problems. Here, we apply the multigrid technique to a nonlinear problem: anisotropic diffusion of digital images.

Let

$$\boldsymbol{A}(\boldsymbol{I}) = \boldsymbol{F} \tag{5}$$

describe a system of nonlinear equations, where $\boldsymbol{A}(\boldsymbol{I})$ is a nonlinear function on the image $\boldsymbol{I}$, and $\boldsymbol{A}(\boldsymbol{I}), \boldsymbol{I}$ and $\boldsymbol{F}$ have dimensions $N \times N$. Since the precise solution of (5) is assumed to be unknown, an approximate solution image $\boldsymbol{J}$ will be computed.

For approximate solutions to the anisotropic diffusion problem, (2) can be used in a relaxation process as follows:

$$[J(\boldsymbol{x})]_{t+1} \leftarrow \left[J(\boldsymbol{x}) + (1/\Omega) \sum_{d=1}^{\Omega} c_d(\boldsymbol{x}) \nabla J_d(\boldsymbol{x}) \right]_t \tag{6}$$

which defines Jacobi (simultaneous displacement) iteration, where t is the time in terms of the number of complete sweeps. In a Gauss–Seidel framework, we have

$$J(\boldsymbol{x}) \leftarrow J(\boldsymbol{x}) + (1/\Omega) \sum_{d=1}^{\Omega} c_d(\boldsymbol{x}) \nabla J_d(\boldsymbol{x}) \tag{7}$$

since the intensities of the new approximation are used immediately in Gauss–Seidel iteration. Equations (6) and (7) can be interpreted as relaxation methods for a system of equations defined by

$$\boldsymbol{A}(\boldsymbol{I}) = 0. \tag{8}$$

For $\boldsymbol{J}$, the approximation of $\boldsymbol{I}, \boldsymbol{A}(\boldsymbol{J})$ has scalar elements given by

$$A(\boldsymbol{x}) = (1/\Omega) \sum_{d=1}^{\Omega} c_d(\boldsymbol{x}) \nabla J_d(\boldsymbol{x}). \tag{9}$$

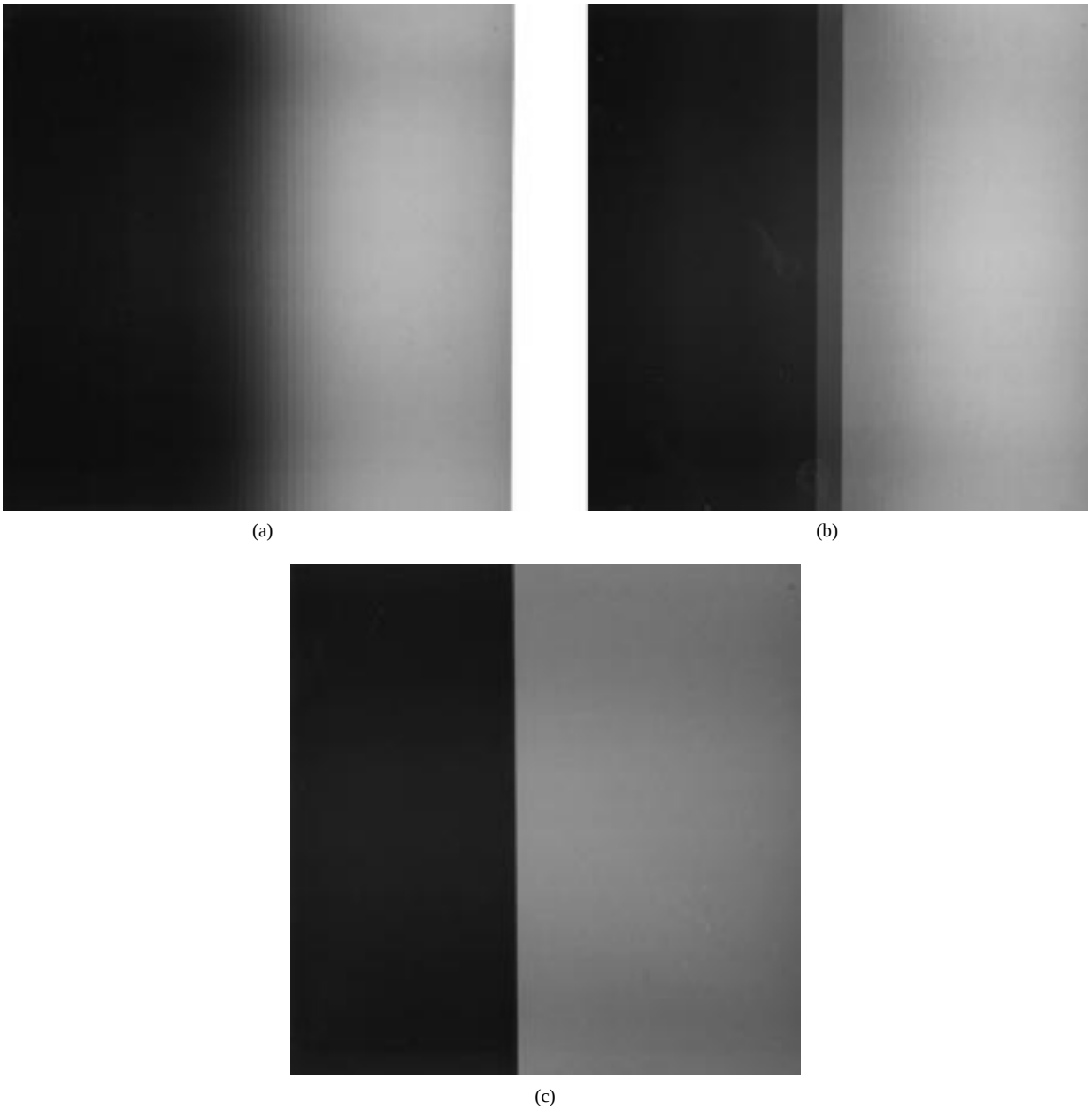

(a) (b)

(c)

Fig. 1. (a) Original sigmoidal ramp edge. (b) After anisotropic diffusion with DC 1 ($k = 10$). (c) After multigrid anisotropic diffusion with DC 1 ($k = 10$).

The algebraic error of the approximation $\boldsymbol{J}$ is defined as

$$\boldsymbol{E} = \boldsymbol{I} - \boldsymbol{J}. \tag{10}$$

Since $\boldsymbol{I}$ is unknown, $\boldsymbol{E}$ is also unknown and inaccessible during the process of computing a suitable $\boldsymbol{J}$. Traditionally, in this case, the residual $\boldsymbol{R}$ has been used to measure the goodness of the approximation $\boldsymbol{J}$. $\boldsymbol{R}$ may be computed during relaxation and is

$$\boldsymbol{R} = \boldsymbol{F} - \boldsymbol{A}(\boldsymbol{J}). \tag{11}$$

For a problem with a unique solution, $\boldsymbol{R} = 0$ if and only if $\boldsymbol{E} = 0$. Note that You *et al.* have presented well-posed formulations of anisotropic diffusion with unique solutions in [21]. Even in the cases where $\boldsymbol{A}(\boldsymbol{I}) = \boldsymbol{F}$ is not well-posed, the norm of $\boldsymbol{R}$ provides a good measure of how well an image $\boldsymbol{J}$ satisfies the system of nonlinear equations in (5).

In using the residual to correct the estimate of $\boldsymbol{I}$, two cases must be examined, the case of linear $\boldsymbol{A}(\cdot)$ and the case of nonlinear $\boldsymbol{A}(\cdot)$. Given a linear function $\boldsymbol{A}(\cdot)$, (11) can be arranged to form

$$\boldsymbol{A}(\boldsymbol{J}) = \boldsymbol{F} - \boldsymbol{R}. \tag{12}$$

Subtracting (12) from (5), the relationship

$$\boldsymbol{A}(\boldsymbol{E}) = \boldsymbol{R} \tag{13}$$

is attained, which is the residual equation. A solution to (13) could be used to correct error in the approximation $\boldsymbol{J}$.

After computing an approximate solution $\boldsymbol{J}$, the residual can be computed using (11). Then, a solution to residual equation can be generated. The resulting estimate of $\boldsymbol{E}$ can be used to correct $\boldsymbol{J}$, since

$$\boldsymbol{I} = \boldsymbol{J} + \boldsymbol{E}. \tag{14}$$

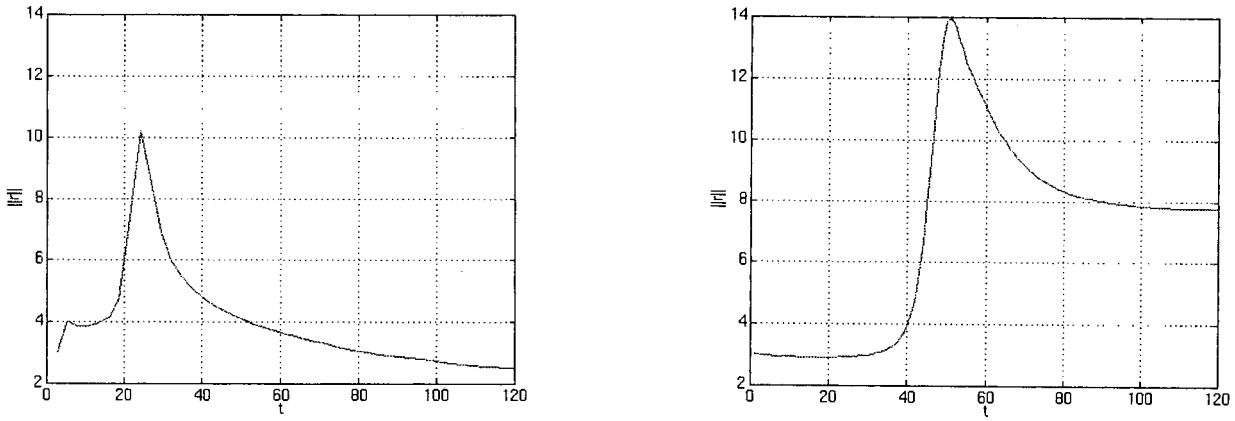

(a) (b)

Fig. 2. (a) Norm of residual versus time using anisotropic diffusion [corresponding to result in Fig. 1(b)]. (b) Norm of residual versus time using multigrid anisotropic diffusion [corresponding to result in Fig. 1(c)]. Time is expressed in work units—the amount of computation required to perform one iteration of anisotropic diffusion.

Thus far, the discussion has not included multiple resolutions. Intergrid transfer functions can be used to move vectors (2-D matrices in the image processing case) between grids of different resolutions. Interpolation operators move a vector from a coarse grid to the next finer grid. The restriction operators move vectors from fine grids to coarse grids. Let $(\cdot)_{\uparrow 2}$ denote interpolation and $(\cdot)_{\downarrow 2}$ denote restriction, for the case where a fine grid has twice as many samples in each linear dimension as the next coarser grid. Also, let l denote the multigrid level, where level $l = 0$ is the original image at full resolution and level $l = \log_2 N$ is the grid with one point. For example, $(\boldsymbol{E}_l)_{\uparrow 2}$ is the interpolation of the error at level l and has same number of grid points as $\boldsymbol{J}_{l-1}$. The selection of the appropriate intergrid transfer functions will be discussed in Section IV.

It was stated earlier that multigrid methods are effective in reducing low-frequency error that may cause significant image artifacts. If a smoothly varying error is subsampled, the error appears more oscillatory. So, the subsampled error can be smoothed using the original system of equations (which essentially eliminates oscillatory behavior). Then, the smooth modes in the error can be eliminated and the original estimates corrected.

B. Coarse Grid Correction (Linear Case)

For the linear case, combining (11) and (13) at level l and transferring to the coarser grid at level $l+1$, we have

$$\boldsymbol{A}(\boldsymbol{E}_{l+1}) = (\boldsymbol{F}_l)_{\downarrow 2} - \boldsymbol{A}[(\boldsymbol{J}_l)_{\downarrow 2}]. \tag{15}$$

Note that $(\boldsymbol{F}_l)_{\downarrow 2} = 0$ for the anisotropic diffusion problem formulated by (8) and (9). Using (15) with initial estimate $\boldsymbol{E}_{l+1} = 0$, the error can be estimated. In fact, relaxing on the original equation (5) with arbitrary initial solution $\boldsymbol{J}$ is the equivalent to relaxing on the residual equation (13) with initial estimate $\boldsymbol{E} = 0$ [7]. A simple two-level multigrid method involves relaxation on (8) with initial estimate $\boldsymbol{J} = \boldsymbol{G}$, transfer of the residual to the coarse level, relaxation on the residual equation (13) at the coarse level with initial estimate $\boldsymbol{E}_{l+1} = 0$, and finally correction on the fine level via interpolation of the error. Given the error estimate computed by relaxing (13), the correction scheme for the estimate at level l is expressed

$$\boldsymbol{J}_l \leftarrow \boldsymbol{J}_l + (\boldsymbol{E}_{l+1})_{\uparrow 2}. \tag{16}$$

C. Coarse Grid Correction (Nonlinear Case)

Because the anisotropic diffusion problem involves a nonlinear function $\boldsymbol{A}(\cdot)$, (13) does not hold, and additional steps must be taken to estimate the error and perform correction. Of course, the nonlinear function $\boldsymbol{A}(\cdot)$ may be assumed to be locally linear, and the additional steps could be ignored. Or, a global linearization step may be used in combination with a Newton method to solve for the error iteratively [6]. Here, the *full approximation scheme* (FAS) is employed for the anisotropic diffusion problem [11]. FAS minimizes the computational effort by avoiding a global linearization step. Given (8), (10), and (11), we have

$$\boldsymbol{A}(\boldsymbol{J} + \boldsymbol{E}) - \boldsymbol{A}(\boldsymbol{J}) = \boldsymbol{R} \tag{17}$$

for the anisotropic diffusion problem. If (17) is transferred from level l to a coarser grid at level $l+1$, we have

$$\boldsymbol{A}[(\boldsymbol{J}_l)_{\downarrow 2} + (\boldsymbol{E}_l)_{\downarrow 2}] = \boldsymbol{A}[(\boldsymbol{J}_l)_{\downarrow 2}] + (\boldsymbol{R}_l)_{\downarrow 2}. \tag{18}$$

Let

$$\hat{\boldsymbol{J}}_{l+1} = (\boldsymbol{J}_l)_{\downarrow 2} + (\boldsymbol{E}_l)_{\downarrow 2}, \tag{19}$$

and

$$\hat{\boldsymbol{F}}_{l+1} = \boldsymbol{A}[(\boldsymbol{J}_l)_{\downarrow 2}] + (\boldsymbol{R}_l)_{\downarrow 2}. \tag{20}$$

Now, we can relax on

$$\boldsymbol{A}[\hat{\boldsymbol{J}}_{l+1}] = \hat{\boldsymbol{F}}_{l+1} \tag{21}$$

with initial estimate $\hat{\boldsymbol{J}}_{l+1} = (\boldsymbol{J}_l)_{\downarrow 2}$. Note that (21) has the same form as (5), so the same relaxation methods can be utilized. Using the estimate of $\hat{\boldsymbol{J}}_{l+1}$ computed via relaxation on (21), the error is computed by

$$\boldsymbol{E}_{l+1} = \hat{\boldsymbol{J}}_{l+1} - (\boldsymbol{J}_l)_{\downarrow 2} \tag{22}$$

and (16) may be used for correction as with the linear case.

D. Multigrid V-Cycle

To this point, only two-level correction methods have been introduced. One may notice that computation of the error at a coarse level has the same form as the original problem. So, it is logical to repeat this correction process and compute the error at the next coarse level to correct the error estimate itself. This process can be continued recursively until a level with an exact solution is reached. Finally, the error corrections can be propagated back to the original resolution. This is called the multigrid V-cycle, as the algorithm starts with an initial estimate, telescopes down to the coarsest grid, and then returns in order to the finest grid [7]. The so-called *full multigrid V-cycle* starts with the exact solution at the coarsest grid and then performs a succession of nested V-cycles to obtain a solution at the finest grid. Full multigrid is valuable when no informed initial estimate is available. Because the anisotropic diffusion problem here relies on an initial estimate (the initial image), the full multigrid V-cycle is not appropriate, and the V-cycle method is utilized.

The multigrid anisotropic diffusion algorithm commences with relaxation on the initial image and proceeds with error correction until the level with just one pixel is reached (one grid point). At this level, the error is set to zero, since the diffusion equations are satisfied for any solution. Alternatively, error correction can be halted at the level below the apex (with four pixels in the 2-D case), without any undesirable effects. The algorithm then returns to the finest level.

The V-cycle multigrid anisotropic diffusion technique is implemented as follows.

- *At Level 0*: Relax on (8) ν times with the initial estimate $\boldsymbol{J} = \boldsymbol{G}$, where $\boldsymbol{G}$ is the original (possibly corrupted) image.
- *At Level 1 to Level* $\log_2(N) - 1$ *(in Ascending Order)*: Relax on (15) (linear case) or (21) (nonlinear case) n times with the initial error estimate $\boldsymbol{E_l} = 0$.
- *At Level* $\log_2(N)$: Set error to $\boldsymbol{E}_{\log_2 N} = 0$.
- *At Level* $\log_2(N) - 1$ *to Level 0 (in Descending Order)*: Correct estimates using (16), then relax ν times at each level.

IV. Analysis and Discussion

Section III presented the multigrid anisotropic diffusion algorithm for adaptive image smoothing. In this section, the algorithm and its implementation are analyzed. First, intergrid transfer functions and relaxation techniques for multigrid anisotropic diffusion are suggested. Then, three variations of the diffusion coefficient are introduced, and guidelines on boundary conditions are given. Finally, the storage requirements, computational cost, and the solution quality of the multigrid method are discussed.

A. Intergrid Transfers

There are several options for the intergrid transfer functions [11], [12]. The main division in the fine-to-coarse transfers is between injection and full-weighting. An injection operator should be familiar to those acquainted with image processing, since it is simply a sampling scheme. Full-weighting methods, on the other hand, use a linear combination of the finer samples to produce a coarse grid point value. Because injection is superior in preserving step edges, the injection operator has been employed in this multigrid method. For the 2-D solution $\boldsymbol{J}$ at level l, injection is given by

$$J_l(x, y) = J_{l-1}(2x, 2y) \tag{23}$$

where x and y are row and column, respectively.

With coarse-to-fine transfers, traditional interpolation techniques can be implemented, or a simple "sample and hold" prolongation strategy can be used. It must be noted that interpolation introduces additional smoothing, which may violate the intent of anisotropic diffusion. Therefore, the prolongation approach is applied, although no perceivable difference in solution quality has been observed between the two operators. Prolongation is achieved via

$$J_l(x, y) = J_{l+1}[\mathrm{int}(x/2), \mathrm{int}(y/2)] \tag{24}$$

where $\mathrm{int}(\cdot)$ is an integer-range truncation function.

B. Relaxation

The choice of the relaxation method for the discrete anisotropic diffusion problem is important in both the traditional and multigrid solutions. The Jacobi (6) and Gauss–Seidel (7) iterates have been introduced. Because the solutions at each grid point (at each pixel site) are replaced simultaneously with the Jacobi approach, oscillatory behavior can occur and convergence rates can be reduced. The Gauss–Seidel approach can be utilized, but, unlike the Jacobi iterates, the Gauss-Seidel iterates are affected by the order of replacement. For the anisotropic diffusion problem, streaking artifacts have been observed when sequential updating is used. This can be alleviated by utilizing a *red-black* update scheme on each row, and a *zebra* scheme on the columns [7]. Simply stated, the grid sites at even columns and even rows are computed, then those with odd rows and odd columns, then odd rows and even columns, and finally even rows with odd columns. This Gauss–Seidel update scheme is used for all results produced in Section V.

It must also be observed that a Gauss–Seidel–Newton method can be used for nonlinear problems [11]. In this case, (7) is replaced by a single Newton iteration, as follows:

$$J_t(\boldsymbol{x}) \leftarrow J(\boldsymbol{x}) - \frac{A(\boldsymbol{x})}{\dfrac{\partial A(\boldsymbol{x})}{\partial J(\boldsymbol{x})}} \tag{25}$$

where $A(\boldsymbol{x})$ is computed using (9).

C. Diffusion Coefficients

To achieve relaxation, a diffusion coefficient must be chosen. As mentioned earlier, three classes of diffusion coefficients are used here. The three (discrete domain) diffusion coefficients are summarized as follows.

Diffusion Coefficient 1: Perona and Malik [14] suggested

$$c_d(\boldsymbol{x}) = \exp\left\{-\left[\frac{\nabla I_d(\boldsymbol{x})}{k}\right]^2\right\} \tag{26}$$

as a diffusion coefficient (DC) , where $c_d(\boldsymbol{x})$ is the DC for location $\boldsymbol{x}$ in diffusion direction d. $\nabla I_d(\boldsymbol{x})$ is the gradient (typically a simple difference) associated with location $\boldsymbol{x}$ and direction d. A method for selecting k is discussed in [1]. The advantages of DC 1 include the ability to sharpen edges (backward diffusion), inexpensive implementation, and rapid smoothing. The disadvantages include the inability to reject outliers (especially in the presence of impulse noise) and the creation of "staircase" artifacts, as documented in [19] and [22]. You *et al.* have also shown that DC 1 leads to an ill-posed problem, where a small perturbation in the data may cause a significant change in the final result [21]. Furthermore, DC 1 does not lead to a unique optimal solution [21].

Diffusion Coefficient 2: Catte *et al.* [9] and Alvarez *et al.* [5] proposed a modification to DC 1 that utilizes a Gaussian-convolved version of the image to compute the diffusion coefficient. The idea is implemented here using the same form as DC 1 and is

$$c_d(\boldsymbol{x}) = \exp\left\{-\left[\frac{\nabla S_d(\boldsymbol{x})}{k}\right]^2\right\} \tag{27}$$

where

$$\boldsymbol{S} = \boldsymbol{I} * \boldsymbol{G}(\sigma). \tag{28}$$

$\boldsymbol{G}(\sigma)$ is a Gaussian kernel with standard deviation σ. The main advantage of DC 2 is improved performance in removing outliers, while maintaining the smoothing rate of DC 1. The use of the smoothed image in the computation of the diffusion coefficients can produce well-posed diffusion that converges to a unique result, under certain conditions [9]. However, it is noted in [21] that algorithms that utilize coefficients such as DC 2 actually contain an isotropic diffusion process, which adds to the computational burden and is against the spirit of anisotropic diffusion.

A morphological variant of DC 2 can be formed by replacing (28) with

$$\boldsymbol{S} = (\boldsymbol{I} \circ \boldsymbol{B}) \bullet \boldsymbol{B} \tag{29}$$

where $\boldsymbol{B}$ is a structuring element of size $m \times m$, $\boldsymbol{I} \circ \boldsymbol{B}$ is the morphological opening of $\boldsymbol{I}$ by $\boldsymbol{B}$, and $\boldsymbol{I} \bullet \boldsymbol{B}$ is the morphological closing of $\boldsymbol{I}$ by $\boldsymbol{B}$. Early results show that (29) allows effective elimination of impulse noise with improved edge preservation.

Diffusion Coefficient 3: Posing anisotropic diffusion as an optimization problem, You *et al.* [21] introduced the following diffusion coefficient:

$$c_d(\boldsymbol{x}) = \begin{cases} 1/T + p(T+\varepsilon)^{p-1}/T, \nabla I_d(\boldsymbol{x}) < T \\ 1/|\nabla I_d(\boldsymbol{x})| + p(|\nabla I_d(\boldsymbol{x})| + \varepsilon)^{p-1}/ \\ \qquad |\nabla I_d(\boldsymbol{x})|, |\nabla I_d(\boldsymbol{x})| \geq T \end{cases} \tag{30}$$

where $\varepsilon > 0$ and $0 < p < 1$. T is a threshold on the gradient magnitude, similar to k in DC 1. DC 3 can avoid the "staircase" effects with sufficient iteration. Also, with a large number of iterations, impulse noise can be eliminated with DC 3. The main drawback is computational expense. Smoothing progresses slowly with DC 3, as demonstrated in the results.

D. Boundary Conditions

Another choice in relaxation with a system of partial differential equations concerns the boundary conditions. It is not logical in the anisotropic diffusion problem to set the border pixels as boundary conditions. The other choices include zero-padding, assuming a periodic image (wraparound), and assuming values beyond the border are equivalent to the border values. As zero-padding and wraparound lead to undesirable false discontinuities, the third approach is utilized. Computation of (7) is achieved at the borders by allowing values beyond the border to be equal to the border value that is being relaxed.

E. Storage Requirements

In time-critical applications, the system architecture may also be limited and storage requirements must be considered. At first glance, the storage requirements for the multigrid implementation may appear to be immense, but this is not the case. For the multigrid V-cycle, the solution and the right hand side variables must be stored at each level above the original grid. On the original $N \times N$ grid, only the solution is stored, since the right hand side is zero for anisotropic diffusion. So, the number of scalar variables S that are stored for the 2-D anisotropic diffusion problem is

$$\begin{aligned} S = {} & N^2 + 2(N^2/2^2 + N^2/2^4 + N^2/2^6 \\ & \cdots + N^2/2^{2\log_2 N}) \end{aligned} \tag{31}$$

and

$$S < (5/3)N^2 \tag{32}$$

which is less than twice the number of pixels in the original image.

F. Computational Expense

The fundamental difference between the efficiency of multigrid anisotropic diffusion and the efficiency of fine grid anisotropic diffusion is that multigrid gives a convergence rate that is independent of the size of the image [17]. For fine grid relaxation schemes (e.g., Jacobi or Gauss–Seidel), the rate of convergence deteriorates as the number of pixels increases. Low-frequency error will be reduced at a rate of $1 - O(1/N^2)$ with the basic iterative schemes [17], whereas multigrid provides an overall convergence rate of $\mu^{2\nu}$ (independent of signal size) [12], where μ is the convergence rate for a damped Jacobi method ($\mu \approx 2/3$), and ν is the number of relaxation steps per multigrid level (typically $\nu = 1$). Hence, for the anisotropic diffusion of digital images, the multigrid approach is strongly motivated.

Although convergence is determined by the specific relaxation method and DC used, some guidelines for the number

of operations required can be given. In general, convergence can be described as

$$||\boldsymbol{E}|| = ||\boldsymbol{I} - \boldsymbol{J}|| < \delta. \tag{33}$$

To reduce the algebraic error from $O(1)$, the error in an arbitrary guess, to $O(1/N^2), O(\log_2 N^2)$ V-cycles are required [7]. Because a single V-cycle has a cost of $O(N^2)$ updates, $O(N^2 \log_2 N^2)$ updates are required for convergence.

The comparison between the convergence behavior of fine grid anisotropic diffusion and multigrid anisotropic diffusion is difficult, because some diffusion implementations will diverge [21], [22]. Given a diffusion coefficient and parameters that lead to convergence, Chen [10] provided a "rule of thumb" for diffusion convergence of $8/w$ iterations/pixel, where w ranged from 0.01 to 0.05. In other words, hundreds of iterations are required to achieve equilibrium. Using Chen's empirical results, $O(8N^2/w)$ updates are needed for anisotropic diffusion on a fine grid, as opposed to the $O(N^2 \log_2 N^2)$ updates for multigrid convergence. The difference gives the multigrid approach at least one order of magnitude improvement in computational cost for typical images. A more formal convergence result was given by Nordstrom [13]. For a restricted (convergent) version of anisotropic diffusion, it was shown that the updates converge *exponentially* [13, Lemma 8.3]. The empirical results of [13] showed that although the exponential rate is conservative, more than 100 sweeps were required on a fine grid. For convergence to the level of truncation (to an error of $O(1/N^2)$) on a 256 $\times$ 256 image, our experiments showed that the multigrid algorithm improved upon the fine grid computational expense by an order of magnitude.

The contrast between the efficiency of fine grid anisotropic diffusion and multigrid anisotropic diffusion can be illustrated by a brief mathematical analysis of two simple signals. Consider two 1-D signals—an impulse of height αk and a double impulse (of width 2) and height αk. Both the single impulse and the double impulse are embedded in a 1-D signal $\boldsymbol{J}$ of length N and are located at $x = N/2$. So, the impulse has $J(N/2) = \alpha k$ and the double impulse has $J(N/2) = J(N/2+1) = \alpha k$ and $J(x) = 0$ otherwise. The rate at which the fine grid anisotropic diffusion process removes these two features is markedly different. Let the condition for feature removal be a reduction in feature height to less than ε (so that $|J(x)| < \varepsilon \; \forall x$), which is to say that all signal differences are reduced such that $|\nabla J_d(x)| < \varepsilon \; \forall d, x$ given that $J(x) \geq 0 \; \forall x$. For the single impulse, the value of $\boldsymbol{A}$ at location $x = N/2$ (given by (9) with $\Omega = 2$) is

$$A(N/2) = -\alpha k \tag{34}$$

using DC 2 with (29) and a structuring element $\boldsymbol{B}$ of width $m = 2$. At each side of the impulse, we have

$$A(N/2-1) = A(N/2+1) = \alpha k/2. \tag{35}$$

The diffusion of this signal proceeds as an isotropic diffusion since $\nabla S_d(x) = 0 \; \forall x, d$ due to the open-close operation of (29). Thus, reduction of the impulse signal is equivalent to the successive convolution with the kernel [1/2 0 1/2]. The maximum value in the resultant sequence at iteration t (for even integer t) is given by

$$\sup[J(x)\colon 0 \leq x \leq N-1] = \frac{\alpha k(t!)}{2^t \left(\frac{t}{2}!\right)^2}. \tag{36}$$

So, the condition for convergence becomes

$$\frac{\alpha k(t!)}{2^t \left(\frac{t}{2}!\right)^2} < \varepsilon. \tag{37}$$

Both multigrid anisotropic diffusion and fine grid anisotropic diffusion reduce this pulse (high-frequency error) in a rapid manner by simple relaxation at the highest resolution. For example, consider an impulse of initial height $J(N/2) = 6.0$ with $\alpha = 3$ and $k = 2$; (37) suggests that only $T = 24$ fine grid iterations are needed to reduce the impulse to a height below unity ($\varepsilon = 1$).

Examining the results for a feature with the same height, but with greater width (the double impulse), the results are quite different. Let $\mu(t)$ represent the convergence rate (the rate of reduction) of the maximum value in $\boldsymbol{J}$ at iteration t. Note that the open-close operation of (29) leaves the gradients unchanged in this case (as does DC 1). So, after the first relaxation step, the double impulse is reduced by a factor of

$$\mu(1) = 1 - \exp(-\alpha^2). \tag{38}$$

Subsequent iteration yields

$$\mu(t+1) \geq 1 - \exp\left[-\frac{J^2(x_m)}{k^2}\right] \tag{39}$$

where x_m is the position of the maximum value in $\boldsymbol{J}$ at iteration t. A necessary, but not sufficient, condition on the number of iterations T needed to reduce the signal such that $|J(x)| < \varepsilon$ is

$$T \geq \min\left\{\tau\colon \alpha k \prod_{t=1}^{\tau} \mu(t) < \varepsilon\right\}. \tag{40}$$

With the double impulse of initial height $J(N/2) = J(N/2+1) = 6.0$, over 524 iterations are required with the fine grid implementation!

For simplicity, consider a two-grid multigrid implementation based on (15). The multigrid anisotropic diffusion technique immediately reduces the difficult double impulse problem to the single impulse problem by a grid transfer. On the first iteration, we have $A((\boldsymbol{J}_0)_{\downarrow 2})(N/4) = E_1(N/4) = -\alpha k, A((\boldsymbol{J}_0)_{\downarrow 2})(N/4-1) = \alpha k/2$, and $A((\boldsymbol{J}_0)_{\downarrow 2})(N/4+1) = \alpha k/2$. When transferred to the coarse grid, the double impulse is eliminated in the same manner as the single impulse. The sequence converges according to (37), and for the example with height $J(N/2) = J(N/2+1) = 6.0$, only 24 multigrid iterations are needed, as opposed to over 524 fine grid iterations. This exemplifies the strength of the multigrid technique and the inability of the fine grid method to eliminate lower frequency error.

For the experimental results, the comparison of computational expense between the fine grid approach and the multigrid method is best evaluated by work units. A work unit is essentially the amount of computation required for a single relaxation sweep at the original image resolution. One iteration

(a) (b)

(c) (d)

Fig. 3. (a) Original "eye" image; (b) corrupted image (Laplacian noise, SNR = 9 dB) used as input for results in (c) and (d); (c) after two iterations of anisotropic diffusion with DC 2 $(k = 25)$; (d) After one iteration of multigrid anisotropic diffusion with DC 2 $(k = 25)$.

of anisotropic diffusion on the (fine grid) image requires one work unit. For the multigrid V-cycle, the number of work units w required is

$$w = 2\nu(N^2 + N^2/2^2 + N^2/2^4 + N^2/2^6 \cdots + N^2/2^{2\log_2 N}) \text{ work units} \quad (41)$$

since each level is visited 2ν times. For a V-cycle with one sweep $(\nu = 1)$ per level

$$w < (8/3) \text{ work units.} \quad (42)$$

Hence, one V-cycle requires less than 8/3 the computation required for one sweep of the standard anisotropic diffusion technique. For the comparisons in Section V, computational expense (time) is measured in work units.

Selection of ν can be fixed [7] (usually at $\nu = 1$) or accommodative [7], [11]. In the accommodative scheme, residuals are computed after each relaxation sweep and used in conjunction with the following stopping rule:

$$\|\boldsymbol{R}_{t+1}\| > \eta \|\boldsymbol{R}_t\| \quad (43)$$

which measures the effectiveness of the relaxation step. For 2-D problems, $\eta = 0.6$ is suggested in [7].

G. Solution Quality

As with most image processing applications, solution quality can be evaluated qualitatively and quantitatively. For qualitative comparisons between the standard anisotropic diffusion implementation and the multigrid method, both high- and low-frequency error can be observed. High-frequency error includes the lack of impulse rejection or edge preservation. Low-frequency error is manifested as blotches, false regions, and wavy backgrounds.

(a) (b) (c) (d)

Fig. 4. (a) Original cameraman image; (b) corrupted image (Laplacian noise, SNR = 13 dB) used as input for results in (c)–(f) and Fig. 5(a) and (b); (c) after eight iterations of anisotropic diffusion with DC 1 ($k = 25$); (d) after eight iterations of anisotropic diffusion with DC 2 ($k = 25$).

To compare the traditional fine grid relaxation approach with the multigrid method in a quantitative manner, the most appropriate measure is the norm of the residual. The norm of the residual evaluates to degree to which the anisotropic diffusion equations (8)–(9) are satisfied. In Section V, the L_2 norm, is applied to measure $\boldsymbol{R}$ as follows:

$$||\boldsymbol{R}|| = \sqrt{\sum_{i=0}^{N-1}\sum_{j=0}^{N-1} R^2(i,j)}. \tag{44}$$

V. Results and Conclusions

In this section, results are given that demonstrate the performance of the multigrid anisotropic diffusion method on digital imagery. The main benefits of using the multigrid approach are the reduction of the computational expense of diffusion and the rapid elimination of low-frequency error. Both of these contributions can be observed by diffusing a synthetically created 2-D ramp edge. A ramp edge can be modeled in 1-D by the sigmoid defined by

$$I_t(x) = \frac{A}{2}\tanh(fx+\theta) + B \tag{45}$$

where A is the magnitude of the edge, f dictates the edge rate of change, θ is the edge displacement, and B is the baseline value of the edge. The inflection point (the center) of the edge is at $x_{ip} = -q/f$. Fig. 1(a) shows a 64 × 64 image

(e) (f)

Fig. 4. (*Continued.*) (e) After eight iterations of anisotropic diffusion with DC 3 ($T = 25, \varepsilon = 1, p = 0.5$); (f) after three iterations of multigrid anisotropic diffusion with DC 2 ($k = 25$).

in which the rows are identical 1-D signals governed by (45), with $A = 100, B = 120, f = 0.1$, and $\theta = -3.2$.

The image shown in Fig. 1(b) is the result of fine grid anisotropic diffusion using DC 1 with $k = 10$. The image in Fig. 1(c) is the result of multigrid anisotropic diffusion using DC 1 with $k = 10$. Note that a false region was created by fine grid anisotropic diffusion and avoided by the low-frequency smoothing of multigrid anisotropic diffusion. Both methods were iterated until the updates became insignificant (<1% change between iterations). The norm of the residual for both methods is shown in Fig. 2, with time expressed in work units. In this case, the norm of the residual is equal to the norm of $\boldsymbol{A}(\boldsymbol{J})$, since $\boldsymbol{R} = -\boldsymbol{A}(\boldsymbol{J})$ for anisotropic diffusion. Each iteration of fine grid anisotropic diffusion is one work unit, but each iteration of the multigrid implementation is expressed as 8/3 work units, due to (42).

The graphs in Fig. 2 show that the multigrid method is able to rapidly reduce the norm of the residual [Fig. 2(b)], while the fine grid anisotropic diffusion method becomes stuck in a locally optimal solution that corresponds to the "staircase" artifact [Fig. 2(a)]. The standard fixed-resolution algorithm actually yields a residual with a larger magnitude than the residual of the initial image. The peak in both graphs can be interpreted as follows: As the anisotropic diffusion of the smooth sigmoid commences, the neighboring signal samples are close in value and diffusion progresses slowly. The rate of diffusion increases as the sigmoid is transformed into a piecewise constant signal. This increase is halted when a step edge of sufficient height to inhibit diffusion has evolved. Then, intraregion smoothing continues until equilibrium has been achieved. However, the equilibrium state of the multigrid implementation yields a residual that is four times smaller than that given by the fine grid implementation.

On real imagery, low-frequency error appears as false regions in the smoothed result. Fig. 3(b) is a corrupted version of the 64× 64 image in Fig. 3(a), where Laplacian-distributed noise—signal-to-noise ratio (SNR) = 9 dB—has been added. When two iterations of fine grid anisotropic diffusion are performed on Fig. 3(b), several blotch artifacts are revealed, as depicted in Fig. 3(c). After just one iteration of multigrid anisotropic diffusion, the false regions have been subdued [Fig. 3(d)]. Note that both solutions utilized the same diffusion coefficient formulation (DC 2 with $k = 25$). For DC 2, a 5 × 5 Gaussian kernel with $\sigma = 1$ was used to compute (28).

The example given in Fig. 4 shows the results that can be obtained by multigrid anisotropic diffusion in just a few iterations. The image in Fig. 4(b) has been corrupted by Laplacian noise (SNR = 13 dB). In Fig. 4(c)–(e), eight iterations of fixed-resolution anisotropic diffusion has been applied to Fig. 4(b), using each one of the three DC's discussed in Section IV. With three iterations of multigrid anisotropic diffusion using DC 2, intraregion smoothing is accomplished [Fig. 4(f)]. Compare the patchy background in Fig. 4(d) with the smooth background in Fig. 4(f), the multigrid result. The outliers shown in Fig. 4(c) and (e) can not be alleviated by the introduction of a multigrid method. The remaining noise in Fig. 4(c) is due to the form of DC 1 [9], [21], and the outliers in Fig. 4(e) are due to insufficient iteration.

With 75 iterations of DC 3, an excellent result is obtained [Fig. 5(a)] that eliminates the impulse noise without destroying important image features. Applying 15 iterations of multigrid anisotropic diffusion with DC 2, interregion smoothing is also achieved [Fig. 5(b)]. For both methods, the number of iterations used represents the fewest number of iterations required to eliminate the majority of the outliers due to the heavy-tailed noise. With the multigrid result [Fig. 5(b)], notice the smoothness of the background and the degree of detail preservation, especially in the face, the camera, and the colonnade of the background building. Although both results in Fig. 5 are visually appealing, the multigrid implementation involves a significantly lower computational cost.

(a) (b)

Fig. 5. (a) After 75 iterations of anisotropic diffusion with DC 3 ($T = 6, \varepsilon = 1, p = 0.5$); (b) after 15 iterations of multigrid anisotropic diffusion with DC 2 ($k = 6$).

In this paper, a multigrid method for performing anisotropic diffusion has been introduced. The multigrid method capitalizes on the multiresolution structure to rapidly eliminate low-frequency error in the diffusion process. The implementation of the multigrid method has been analyzed, and the storage requirements, the computational cost, and the solution quality have been discussed. Results have been provided for synthetic and natural images that show the strengths of the multigrid approach.

Future research includes further analysis of convergence for multigrid anisotropic diffusion and improved methods of forming the original problem. The system of equations described by (8) and (9) has no unique solution. Instead, an initial solution is given by $\boldsymbol{G}$ and diffusion progresses from this starting point. An alternative approach to implementing diffusion involves the use of a data constraint on the solution. The data constraint bounds the distance norm between the solution and the original image. Then (9) takes the form

$$A(\boldsymbol{x}) = (1/\Omega)\sum_{d=1}^{\Omega} c_d(\boldsymbol{x})\nabla J_d(\boldsymbol{x}) + \lambda||J(\boldsymbol{x}) - G(\boldsymbol{x})|| \quad (46)$$

where λ is a regularization parameter. (46) resembles the traditional regularized image restoration approach. Given (46), a full multigrid method could be employed [6]. This approach is currently under investigation.

REFERENCES

[1] S. T. Acton, "Edge enhancement of infrared imagery by way of the anisotropic diffusion pyramid," in *Proc. IEEE Int. Conf. Image Processing*, Lausanne, Switzerland, Sept. 16–19, 1996.

[2] ——, "A pyramidal edge detector based on anisotropic diffusion," in *Proc. IEEE Int. Conf. Acoustics, Speech, Signal Processing (ICASSP-96)*, Atlanta, GA, May 7–10, 1996.

[3] S. T. Acton, A. C. Bovik, and M. M. Crawford, "Anisotropic diffusion pyramids for image segmentation," in *Proc. IEEE Int. Conf. Image Processing*, Austin, TX, Nov. 1994.

[4] S. T. Acton and A. C. Bovik, "Anisotropic edge detection using mean field annealing," in *Proc. IEEE Int. Conf. Acoustics, Speech, Signal Processing (ICASSP-92)*, San Francisco, CA, Mar. 23–26, 1992.

[5] L. Alvarez, P.-L. Lions and J.-M. Morel, "Image selective smoothing and edge detection by nonlinear diffusion II," *SIAM J. Numer. Anal.*, vol. 29, pp. 845–866, 1992.

[6] J. H. Bramble, *Multigrid Methods.* New York: Wiley, 1993.

[7] W. L. Briggs, *A Multigrid Tutorial.* Philadelphia, PA: SIAM, 1988.

[8] M. C. Burton and S. T. Acton, "Target tracking using the anisotropic diffusion pyramid," *Proc. IEEE Southwest Symposium Image Analysis and Interpretation*, San Antonio, TX, Apr. 8–9, 1996.

[9] F. Catte, P.-L. Lions, J.-M. Morel, and T. Coll, "Image selective smoothing and edge detection by nonlinear diffusion," *SIAM J. Numer. Anal.*, vol. 29, pp. 182–193, 1992.

[10] J. Chen, "Generalized adaptive smoothing for multiscale edge detection," in *Proc. SPIE*, vol. 1708, pp. 341–351, 1992.

[11] W. Hackbush and U. Trottenberg, Eds., *Multigrid Methods*. New York: Springer-Verlag, 1982.

[12] S. F. McCormick, Ed., *Multigrid Methods*. Philadelphia, PA: SIAM, 1987.

[13] K. N. Nordstrom, "Biased anisotropic diffusion—A unified approach to edge detection," Dept. Elect. Eng. Comput. Sci., Tech. Rep., Univ. Calif. Berkeley, Berkeley, CA, 1989.

[14] P. Perona and J. Malik, "Scale-space and edge detection using anisotropic diffusion," *IEEE Trans. Pattern Anal. Machine Intell.*, vol. 12, pp. 629–639, 1990.

[15] P. Saint-Marc, J. Chen, and G. Medioni, "Adaptive smoothing: A general tool for early vision," *IEEE Trans. Pattern Anal. Machine Intell.*, vol. 13, pp. 514–529, 1991.

[16] D. Terzopoulos, "Image analysis using multigrid relaxation methods," *IEEE Trans. Pattern Anal. Machine Intell.*, vol. PAMI-8, pp. 129–139, 1986.

[17] P. Wesseling, *An Introduction to Multigrid Methods*. New York: Wiley, 1991.

[18] R. T. Whitaker and G. Gerig, "Vector-valued diffusion," in *Geometry-Driven Diffusion in Computer Vision*, B. ter Haar Romeny, Ed. Boston, MA: Kluwer, 1994, pp. 93–134 .

[19] R. T. Whitaker and S. M. Pizer, "A multi-scale approach to nonuniform diffusion," *Comput. Vis., Graph., Image Process.—Image Understand.*, vol. 57, pp. 99–110, 1993.

[20] A. Yaicharoen and S. T. Acton, "A hybridized edge preservation coefficient for anisotropic diffusion," in *Proc. SPIE Symp. Visual Communications and Image Processing (VCIP-96)*, Orlando, FL, Mar. 17–20, 1996.

[21] Y.-L. You, W. Xu, A. Tannenbaum, and M. Kaveh, "Behavioral analysis of anisotropic diffusion in image processing," *IEEE Trans. Image Processing*, vol. 5, pp. 1539–1553, 1996.

[22] Y.-L.You, M. Kaveh, W. Xu, and A. Tannenbaum, "Analysis and design of anisotropic diffusion for image processing," in *Proc. IEEE Int. Conf. Image Processing*, Austin, TX, Nov. 13–16, 1994.

Scott T. Acton (S'89–M'93) received the B.S. degree in electrical engineering from the Virginia Polytechnic Institute and State University, Blacksburg, in 1988, and the M.S. and Ph.D. degrees in electrical engineering from the University of Texas at Austin, in 1990 and 1993, respectively.

He has been with AT&T, Oakton, VA, the MITRE Corporation, McLean, VA, and Motorola, Inc, Phoenix, AZ. Currently, he is an Associate Professor in the School of Electrical and Computer Engineering, Oklahoma State University (OSU), Stillwater, where he directs the Oklahoma Imaging Laboratory. The laboratory is sponsored by several organizations including the Army Research Office (ARO), NASA, and Lucent Technologies. His research interests include multiscale image representations, diffusion algorithms, image morphology, and image restoration.

Dr. Acton is the winner of the 1996 Eta Kappa Nu Outstanding Young Electrical Engineer Award, a national award given annually since 1936. At OSU, he has been selected as the 1997 Halliburton Outstanding Young Faculty Member. He serves as Associate Editor of the IEEE TRANSACTIONS ON IMAGE PROCESSING and is an active participant in the IEEE, ASEE, SPIE, and Eta Kappa Nu.